A 3400 year lacustrine paleoseismic record from the North Anatolian Fault, Turkey: Implications for bimodal recurrence behavior

Item Type	Article
Authors	Avsar, Ulas; Hubert-Ferrari, Aurélia; Batist, Marc De; Fagel, Nathalie
Citation	A 3400 year lacustrine paleoseismic record from the North Anatolian Fault, Turkey: Implications for bimodal recurrence behavior 2014, 41 (2):377 Geophysical Research Letters
Eprint version	Publisher's Version/PDF
DOI	10.1002/2013GL058221
Publisher	American Geophysical Union (AGU)
Journal	Geophysical Research Letters
Rights	Archived with thanks to Geophysical Research Letters
Download date	02/04/2020 21:05:11
Link to Item	http://hdl.handle.net/10754/552117

A 3400 year lacustrine paleoseismic record from the North Anatolian Fault, Turkey: Implications for bimodal recurrence behavior

Ulaş Avşar[1,2], Aurélia Hubert-Ferrari[3], Marc De Batist[1], and Nathalie Fagel[4]

[1]Renard Centre of Marine Geology (RCMG), Ghent University, Gent, Belgium, [2]Division of Physical Sciences and Engineering, King Abdullah University of Science and Technology (KAUST), Thuwal, Kingdom of Saudi Arabia, [3]Unit of Physical and Quaternary Geography, University of Liège, Liège, Belgium, [4]Department of Geology, University of Liège, Liège, Belgium

Abstract High-resolution physical, geochemical, and geochronological analyses on the sedimentary sequence of Yeniçağa Lake, located in a fault-bounded basin along the North Anatolian Fault, reveal fingerprints of paleoearthquakes. A robust sediment chronology, spanning the last 3400 years, is constructed by radiocarbon dating and time-stratigraphical correlation with the precisely dated Sofular Cave speleothem record. Yeniçağa sedimentary sequence contains 11 seismically induced event deposits characterized by siliciclastic-enriched intervals. Some of the event deposits are also associated with implications of sudden lake deepening, which may be related to coseismic subsidence. The paleoearthquake series having an average recurrence interval of ca. 260 years are interrupted by two possible seismic gaps of ca. 420 and 540 years.

1. Introduction

The collection of paleoseismic data is crucial to understand the long-term patterns of seismicity and to improve seismic hazard assessments. Such data are most commonly obtained from geological records, typically investigated by means of on-fault paleoseismic trenching. Additionally, lacustrine sedimentary sequences can be used as records of paleoseismic events. This has been demonstrated in different tectonic settings, for example, at subduction zones, which generate megathrust earthquakes [e.g., *Moernaut et al.*, 2007] or low deformation areas in the Alps [e.g., *Beck*, 2009; *Strasser et al.*, 2013]. In lacustrine environments, multiple contemporaneous mass-wasting events and/or in situ soft sediment deformations are usually attributed to a seismic triggering mechanism [e.g., *Monecke et al.*, 2006; *Beck*, 2009; *Kagan et al.*, 2011]. In addition, earthquake-induced landslides may increase the sediment yield in the lake catchment [e.g., *Dadson et al.*, 2004], which can be observed in sediment cores retrieved from the lake [e.g., *Leroy et al.*, 2010]. In case of being directly located on the fault, traces of coseismic fluid emissions [e.g., *Ben-Menahem*, 1976] and tectonic subsidence/uplift [e.g., *Bertrand et al.*, 2011] can be found in lacustrine sedimentary sequences. Compared to terrestrial environments, lacustrine environments may contain relatively well preserved, continuous, and long sedimentary archives [e.g., the 50 kyr long record of *Marco et al.*, 1996]. However, unlike the evident seismic origin of events detected by on-fault trenching, sedimentary events in lacustrine sequences may have several triggering mechanisms other than seismic activity, mostly climatic in origin. Therefore, temporal correlation with historical seismicity and/or on-fault trenching data is crucial in order to assign a seismic triggering mechanism to lacustrine sedimentary events.

Here we focus on a lacustrine record obtained along the western part of the North Anatolian Fault (NAF), a major 1000 km long dextral strike-slip fault in Turkey (Figure 1a). The region has an almost 2000 year long well-acknowledged historical record of seismicity [e.g., *Ambraseys*, 2009] and relatively abundant on-fault paleoseismic trenching data [e.g., *Fraser et al.*, 2010]. The fault is characterized by a rapid deformation rate (~20 mm/yr), which was constrained by both GPS measurements [e.g., *Reilinger et al.*, 2006] and geological evidences [e.g., *Hubert-Ferrari et al.*, 2002]. During the 20th century, the stress accumulated on the NAF was released by cascading sequences of M > 7 earthquakes with progressive ruptures from east to west [e.g., *Stein et al.*, 1997]. However, some recent paleoseismic studies argue that the progressive and cascading nature of the 20th century earthquake sequence may not be typical for the long-term behavior of the NAF, and the recurrence interval of earthquakes may not be truly quasi-periodic [*Hartleb et al.*, 2006; *Kozacı*, 2008; *Fraser et al.*,
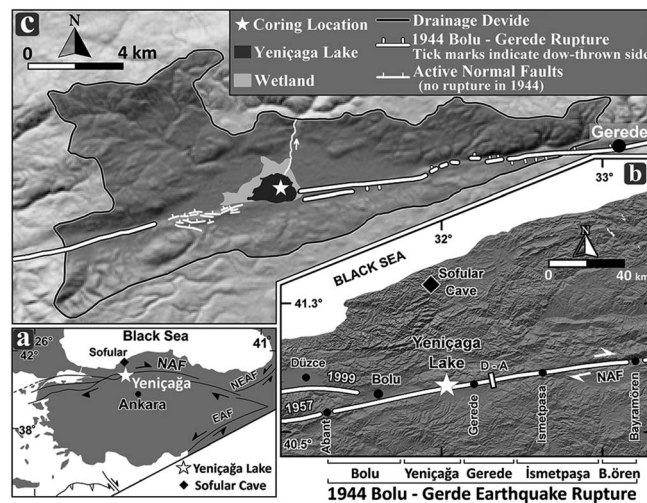
Figure 1. (a) Major tectonic features in Anatolia and the locations of Yeniçağa Lake and Sofular Cave. NAF: North Anatolian Fault, EAF: East Anatolian Fault, and NEAF: Northeast Anatolian Fault. (b) 1944 Bolu-Gerede Earthquake rupture and its segments. Rectangle labeled as "D-A" stands for the Demirtepe [*Kondo et al.*, 2010] and Ardıçlı [*Okumura et al.*, 1993; *Rockwell et al.*, 2006] trench sites. (c) Relief-shaded map of Yeniçağa catchment and the trace of 1944 surface rupture [*Kondo et al.*, 2005].

2010]. Our study aims to provide a long record of paleoearthquakes along the 1944 Bolu-Gerede Earthquake (Ms = 7.3) rupture and to address fundamental questions regarding earthquake recurrence.

2. Study Area

Details of the 1944 Bolu-Gerede Earthquake rupture are provided by *Kondo et al.* [2005], who define five fault segments (Figure 1b). On the Gerede segment, on-fault paleoseismic investigations were conducted at the Demirtepe [*Kondo et al.*, 2010] and Ardıçlı trench sites [*Okumura et al.*, 1993; *Rockwell et al.*, 2006]. Yeniçağa Lake (40.7803°N, 32.0232°E, 989 m a.s.l.), located 20 km to the west of these trench sites, partly fills a fault-bounded basin at the boundary between the Yeniçağa

and Gerede segments. It is a small (2.15 km^2) and shallow (4.5 m) lake, which is surrounded by wetlands, except along its southern margin (Figure 1c). In its catchment (158 km^2), the NAF juxtaposes units of dissimilar age, origin, lithofacies, and internal structure. The area south of NAF is composed of Galatean volcanics, while the area to the north consists of ophiolitic mélange and fluvio-lacustrine sedimentary rocks [*Arca*, 2004].

3. Methods

A 4.6 m long piston core was retrieved from the deepest part of the lake. Inorganic geochemical properties of the sediments along the core were evaluated based on the variations of 22 elements, which are measured by ITRAX micro-XRF core scanner. The measurements were performed with a resolution of 2 mm and 12 s exposure time with the Mo-tube. Radiographic images, which provide information on sedimentary structures and sediment density variations, are obtained by a SCOPIX X-ray image-processing system. The organic matter content was quantified at every 2 cm by weight loss on ignition at 550°C (LOI$_{550}$) and at every 5 cm by total organic carbon (TOC) measurements with an element analyzer. Before the TOC measurements, the samples were dried, ground, and then exposed to fumic HCl acid for 2–3 days in a glass aquarium to remove carbonates. Sediment chronology was constructed by AMS ^{14}C measurements on bulk sediment samples and different organic fractions extracted from the sediments (i.e., phragmite remains, charcoals, pollen, and ephippia of *Daphnia*). The raw radiocarbon dates were calibrated by OxCal 4.0 software [*Bronk Ramsey*, 2007] with the IntCal04 atmospheric curve of *Reimer et al.* [2004]. The radiocarbon chronology was further improved by tuning the Yeniçağa record to the high-resolution δ^{13}C record of Sofular cave [*Fleitmann et al.*, 2009].

4. Sediment Chronology

At the bottom of the core, radiocarbon measurements were made on five different fractions at almost the same depth, which allow interfraction age comparison (Figure 2a). Pollen extract provides the youngest date, implying that the other fractions can be under reworking and/or hard-water effect. At the upper parts of the core, reworking and/or the hard-water effect on bulk and charcoal samples become more obvious; therefore, all ages obtained from these samples can be neglected. Phragmite and ephippia of *Daphnia* samples are in a reasonable chronostratigraphic order along the core. Given that the ages of the samples at the core bottom are older than the pollen extract, they are probably under hard-water effect as well and cannot be directly included into the age-depth model. Preliminarily, a linear age-depth model having a mean sedimentation rate (M.S.R.) of 0.14 cm/yr seems to be the most reasonable chronological model. This rate is also supported
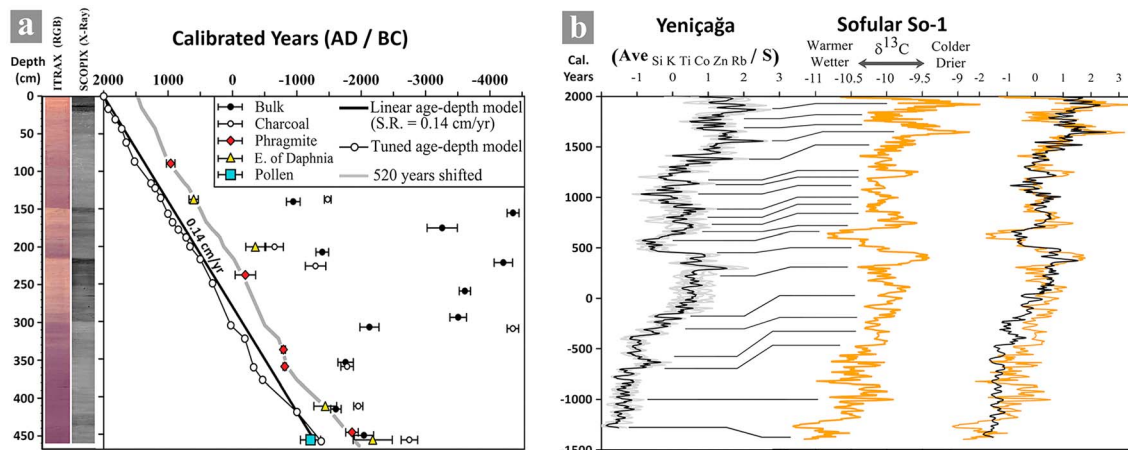
Figure 2. (a) RGB and radiographic images of the core, calibrated radiocarbon dates, and preliminary linear and tuned age-depth models. (b) Tuning of Yeniçağa record to Sofular So-1 δ^{13}C record [*Fleitmann et al.*, 2009]. Horizontal lines represent the tie points between two records. On the rightmost, two records are overlapped after tuning.

by the dates of the lower and upper most phragmite and ephippia of *Daphnia* samples. Phragmite samples at 90 and 448 cm have dates of 960 ± 67 AD and 1858 ± 98 BC, respectively. These dates suggest an M.S.R. between 0.12 and 0.135 cm/yr. Ephippia of *Daphnia* samples at 138 and 458 cm have dates of 604 ± 72 AD and 2180 ± 304 BC, respectively. These samples result in an M.S.R. between 0.10 and 0.13 cm/yr. Accordingly, an M.S.R. of 0.14 cm/yr can be assumed as the preliminary age-depth model.

In order to improve this preliminary model, the Yeniçağa record was tuned to the 50 kyr long precisely dated and highly resolved stalagmite δ^{13}C record from Sofular Cave [*Fleitmann et al.*, 2009] located 70 km to the north of the lake (Figure 1b). First, the Yeniçağa ITRAX data set (FigureS1) was examined to determine a paleoclimatic proxy compatible with the Sofular record. The standardized elemental profiles presented in Figure S1 are peak area values extracted from ITRAX XRF spectra. They are semiquantitative proxies in nature and bear traces of the physical properties of the sediments as well, such as water and organic matter content. In order to eliminate this kind of bias in ITRAX data sets and to evaluate relative changes in the elemental concentrations, interelement ratios are commonly used in paleoenvironmental studies [e.g., *Kylander et al.*, 2011]. The linear age-depth model was assigned to all possible interelement ratios of the Yeniçağa ITRAX data set, and their correlations with the Sofular δ^{13}C record were investigated. The matrix presenting the correlation coefficients is provided in Figure S2. The ratios of the detrital aluminosilicate elements (e.g., Si, K, Ti, Co, Zn, and Rb) to sulfur (S) have relatively higher correlation coefficients with the Sofular δ^{13}C record. Hence, the average of these ratios is tuned to the Sofular δ^{13}C record through the tie points presented in Figure 2b. The tuned records match very well, especially for the period after 300 AD. The warmer and wetter climatic conditions, expressed by more negative δ^{13}C values in the Sofular record, correspond to relatively high S contents in the Yeniçağa record, probably indicating organic S enrichments. The uptake of S by algae and their subsequent sedimentation are the main processes for organic S deposition within lakes, which also reflects the level of primary production [*Urban*, 1994]. Warmer and wetter climatic conditions seem to favor high primary production in Yeniçağa Lake, resulting in organic S enrichments in the sedimentary sequence.

In Figure 2a, the tuned age-depth model is plotted by representing each tie point as a node. It should be remarked that (i) the deviation of the tuned model from the preliminary linear model is usually less than the radiocarbon dating errors, (ii) the approximately 520 year shift on the tuned age-depth model coincides with the floating chronology of phragmite and ephippia of *Daphnia* samples, indicating a probable 520 years of hard-water effect, and (iii) for the period before 500 BC, where the correlation is relatively low, the last two tie points are determined in accordance with the M.S.R. by the dates of phragmite and ephippia of *Daphnia* samples around these depths.

5. Sedimentary Earthquake Record

The Yeniçağa sedimentary sequence contains alternations of homogenous yellowish silty clay and reddish-brown peaty gyttja deposits (Figure 3). Silty clay appears in darker colors on the radiographic image since it has higher density than peaty gyttja, which is dominantly composed of macrofossils of wetland plants
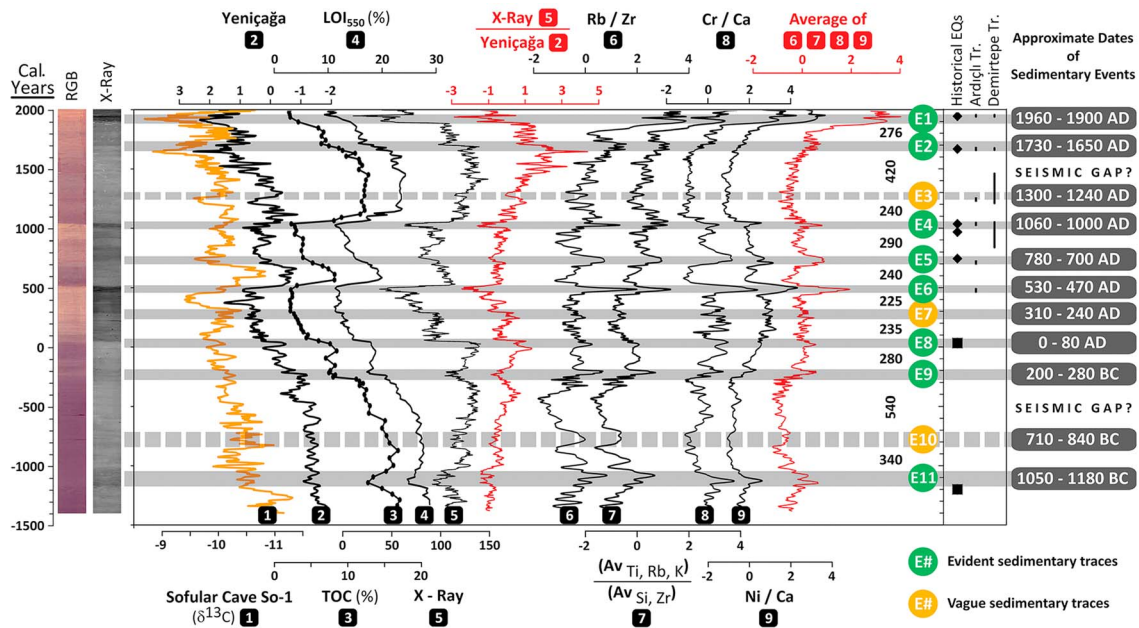
Figure 3. Seismically induced sedimentary events (gray bars) detected in Yeniçağa sequence. All proxies and the core images are adapted to the tuned age-depth model in Figure 2a. Please note the reverse x axis of profiles #1 and #2. Profile #2 is (Ave $_{Si,K,Ti,Co,Zn,Rb}$ / S) ratio of Yeniçağa record.

(e.g., reeds). In general, organic matter content and X-ray gray scale profiles correlate with the XRF paleoclimatic proxy profile (Ave $_{Si,K,Ti,Co,Zn,Rb}$ / S, i.e., profile #2 in Figure 3). The warmer and wetter periods are represented by peaty gyttja, while colder and drier periods by silty clay. It seems that optimal climatic conditions favor not only the primary production in the lake but also the biogenic production in the catchment and wetlands around the lake. Compared to the paleoclimatic proxy profile, the X-ray gray scale profile contains some remarkable anomalies pointing out denser sedimentation episodes, e.g., around 1000 AD. In order to investigate the relation of density variations with the climatic changes, the X-ray gray scale profile is divided by the paleoclimatic proxy profile. The division results in a relatively straight profile confirming that the variations in lithology, as well as in density, are mainly of climatic origin. The division also confirms the existence of sediment intercalations that are denser than expected, e.g., around 500 and 1000 AD. In addition to these intercalations, there are also shifts to more clastic and denser sedimentation, e.g., around 50, 300, and 1700 AD.

The ITRAX data set is further investigated to understand the physical and geochemical properties of the intercalations. Zr and Si are generally associated with coarse-grained fractions and Ti, Rb, and K with clay mineral assemblages. Therefore, their ratios can be interpreted as an indicator of grain size variations [e.g., *Dypvik and Harris*, 2001; *Kylander et al.*, 2011]. Accordingly, Rb/Zr and (Av $_{Ti,Rb,K}$) / (Av $_{Si,Zr}$) profiles (#6 and #7 in Figure 3) indicate that sediment intercalations are enriched in fine-grained siliciclastic material, probably clay minerals. In addition, the intercalations are also enriched in Cr and Ni (profiles #8 and #9), implying increased sediment influx derived from chemical weathering products of mafic and/or ultramafic rocks [e.g., *Wronkiewicz and Condie*, 1989], which are abundant in the catchment of Yeniçağa Lake. The average of the above mentioned grain-size-related profiles (#6, #7, #8, and #9) is also plotted in Figure 3 for an overall representation.

In the light of the above mentioned observations, 11 sedimentary events are detected along the Yeniçağa core (gray bars in Figure 3). All events, except E3, E7, and E10, show evident traces in both profiles, representing the denser, siliciclastic-enriched and fine-grained nature of the sediments (i.e., the red profiles in Figure 3). The possible seismic origin of these sedimentary events is evaluated by comparing the event timing with historical seismicity and on-fault paleoseismic data. Historical seismicity records provide temporally accurate information, but sometimes their spatial accuracy is questionable. In addition, historical records are often incomplete due to changes in various factors through time such as population density, the presence, interest, and motivation of chronologists in the area, as well as social and political circumstances [*Gutdeutsch and Hammerl*, 1999; *Nasir et al.*, 2013]. There are plenty of historical records available in the western part of
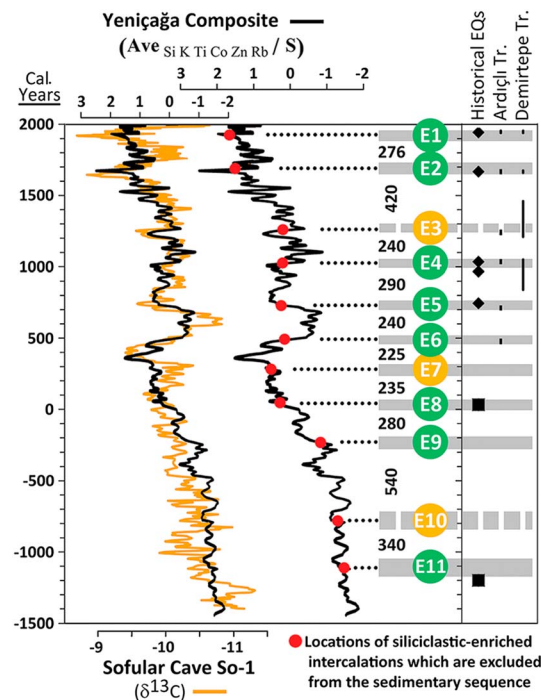
Figure 4. Paleoclimatic proxy record of Yeniçağa Lake (i.e., Ave $_{Si,K,Ti,Co,Zn,Rb}$ / S ratio), after excluding the event deposits and tuning to Sofular So-1 δ^{13}C record. Red dots represent the locations of excluded events deposits. The chronology of the sedimentary events is almost the same as in Figure 3.

the NAF; however, the multistrand and complex nature of this part of the fault often limits the determination of the exact source location. Yet, it is well acknowledged that the Yeniçağa segment ruptured in 1944, 1668, and in 1035 or 967 [e.g., *Ambraseys and Jackson*, 1998; *Kondo et al.*, 2005; *Ambraseys*, 2009]. E1, E2, and E4 coincide with these earthquakes. E5 coincides with the 740 AD earthquake. Even though it is not clear whether this earthquake ruptured the Yeniçağa segment or not, severe damages with a great loss of life were reported in the Roman province called Bithynia [*Ambraseys*, 2009], in which Yeniçağa Lake is also located. E8 matches the 32 AD earthquake documented by *Ambraseys and Jackson* [1998], and E11 coincides with the ~1200 BC earthquake sequence damaging ancient cities in Anatolia [*Nur and Cline*, 2000]. The remaining events were probably large earthquakes too, but they do not appear in the historical records, probably due to the above mentioned issues causing incomplete historical records. Besides the historical seismicity records, six surface rupturing earthquakes were identified at ca. AD 480, 710, 1035, 1235, 1668, and 1944 at Ardıçlı trench site [*Okumura et al.*, 1993; *Rockwell et al.*, 2006]. At Demirtepe trench site, *Kondo et al*. [2010] report the evidences of surface rupturing in ca. AD 960–840, 1460–1210, 1668, and 1944. The youngest six events (E1–E6) in the Yeniçağa core are temporally in good agreement with the on-fault paleoseismic data.

Boes et al. [2010] studied the event deposit of the 1944 Bolu-Gerede earthquake in Yeniçağa Lake. They attribute a denser sediment intercalation, which appears darker in the radiographic images, to the 1944 earthquake. Implications of earthquake-related denser sedimentation are also found in Sapanca Lake, 150 km to the west of Yeniçağa [*Schwab et al.*, 2009; *Leroy et al.*, 2009, 2010].

Fine-grained siliciclastic enrichments in the Yeniçağa record can be attributed to increased erosion in the catchment due to earthquake-induced landslides and/or a seismically shattered landscape [e.g., *Keefer*, 1994; *Keefer and Moseley*, 2004]. Historical records report eyewitness accounts of muddy rivers after earthquakes, e.g., after the 1679 Erivan earthquake [*Ambraseys*, 2009]. This phenomenon is also supported by quantitative analyses of the suspended load of rivers before and after 1999 Mw 7.6 Chi-Chi earthquake in Taiwan [e.g., *Dadson et al.*, 2004]. Seismically induced slope failures and/or shattering on the volcanic units and ophiolithic mélange in the Yeniçağa catchment probably increased the erosion of the chemical weathering products of these units, which are expected to be rich in clay minerals and elements like Cr and Ni.

Sedimentary records of catchment response to seismic activity are relatively rare in the lacustrine paleoseismology literature [e.g., in Lake Pringa by *Howarth et al.*, 2012]. Figure S3 presents a comparison of catchment area to lake area ratios of 52 lakes worldwide [updated from *Avsar*, 2013]. The catchment/lake area ratio of Yeniçağa Lake is 74, where the median is ca. 14 for all of the lakes studied. Undoubtedly, rock type and slope steepness in the catchment as well as climatic conditions in the region are effective parameters in determining the magnitude of catchment response. However, it seems that the relatively big catchment of Yeniçağa Lake allowed the observation of earthquake-triggered increase in sediment yield as distinctive siliciclastic-enriched intervals in the sedimentary sequence.

Some of the events are associated with shifts to denser sedimentation with less organic matter (e.g., E1, E2, E7, and E8), which may imply sudden deepening of the lake due to coseismic subsidence. As the lake gets deeper, the vegetated shores get more distant from the coring location, where only fine-grained terrestrial

organic matter can reach. This results in relatively denser sediments with less organic matter. However, this kind of interpretations requires more detailed investigations on multiple cores in the lake.

The results of *Boes et al.* [2010] on the sedimentary consequences of the 1944 earthquake in Yeniçağa Lake suggest that the sedimentation rate increased by a factor of ca. 50 in the 1940s. Accordingly, the deposition of siliciclastic-enriched intercalations in the Yeniçağa sequence may be instantaneous. In order to consider this possibility and to crosscheck the constructed event chronology, the event deposits represented by gray bars in Figure 3 were excluded from the paleoclimate proxy profile. The resulting composite profile is tuned again to the $\delta^{13}C$ record of Sofular Cave (Figure 4). The red dots on the profile represent the locations of the excluded event deposits. The correlation between Sofular and Yeniçağa records, and the chronology of the events remain almost the same. This observation also suggests that the event deposits are free of climatic impact.

6. Concluding Discussions

In this study, denser siliciclastic-enriched intervals in the Yeniçağa Lake sedimentary sequence are mainly attributed to increased erosion in the catchment due to earthquake-induced landslides and/or a seismically shattered landscape. The record reveals paleo-earthquake series having interevent times ranging mainly between 225 and 340 years. However, two longer interevent times of ca. 420 and 540 years are observed (Figures 3 and 4), which may imply the presence of seismic gaps. Yet, in order to validate this conclusion, two major questions should be answered: (1) Do the lake sediments record only the earthquakes having characteristic magnitudes of the NAF (i.e., M > 7) or do they also record low-magnitude near-field earthquakes and high-magnitude distant earthquakes? (2) Do the lake sediments record all of the large characteristic earthquakes?

Numerous studies, based on the observations on 40 to 60 world-wide earthquakes, have established correlations between the earthquake magnitudes and the occurrences of triggered landslides [e.g., *Keefer*, 1984; *Keefer*, 1994; *Rodriguez et al.*, 1999; *Bommer and Rodriguez*, 2002; *Malamud et al.*, 2004]. *Keefer* [1994], for example, could establish a power law correlation ($r^2 = 0.88$) between the total landslide volume and the moment magnitude, even for earthquakes that occurred in a wide variety of environments. More recently, *Malamud et al.* [2004] confirmed the results of *Keefer* [1994] and proposed that the minimum earthquake magnitude required to trigger landslides is $M_w = 4.3 \pm 0.4$. Although it seems that such low-magnitude earthquakes can trigger landslides, *Keefer* [1994] illustrates the power law correlation by giving an example from Peru and adjacent regions. Accordingly, 99% and 92% of the calculated landslide volume were found to be produced by earthquakes with M > 6 and M > 7, respectively. Additionally, *Keefer* [1984] determined the maximum distance of landslides from the epicenter and fault rupture. For earthquakes having magnitudes of 7.0–7.2, the average maximum distance of landslides from the epicenter is 120–140 km, and 80–100 km from the fault rupture. Based on the outcomes of these empirical studies, we expect that Yeniçağa Lake records only the large earthquakes (M > 7), which take place in its vicinity.

The answer to the second question is less simple. Considering the last 1500 years, the temporal comparison of the Yeniçağa record with the historical seismicity and trenching data implies that the lake consistently records the characteristic large earthquakes on the NAF. However, the sedimentary appearances of E3 and E10 are relatively nondistinct compared to the other events. This may simply indicate that these earthquakes had lower magnitudes (i.e., M ~ 6.0). On the other hand, based on our paleoclimatic interpretation, both events took place during the warmer and wetter climatic episodes, which favor the biogenic production in the catchment and wetlands around the lake. Accordingly, dense vegetation in the catchment would inhibit the increase in erosion due to seismic activity; hence, the sedimentary traces in the lake are expected to be less distinct. This argument implies that the lake sediments may not clearly record earthquakes during high biogenic production episodes. However, the clear appearance of E11, which also took place during a high biogenic production episode, rules this suspicion out. Investigations on longer cores from Yeniçağa Lake, as well as from other fault-bounded basins along the NAF, would be highly useful to inspect the multisite presence and coevality of seismic gaps, as it was successfully done by *Kagan et al.* [2011] on the Dead Sea Fault.

The existence of seismic gaps and/or bimodal recurrence behavior along the NAF was also implied by *Fraser et al.* [2010], who reviewed the on-fault paleoseismological data. They evaluated the long-term behavior of the NAF in terms of probability distribution functions of summed interevent times, which accounts for the natural variability of interevent times and is more representative for the fault behavior [*Lienkaemper and Bronk Ramsey*, 2009]. Accordingly, the western section of the NAF has bimodal recurrence intervals with two

typical lengths of interevent times, ca. 200 and 650 years. Variability in recurrence intervals was also observed in the San Andreas Fault [*Weldon et al.*, 2004]. It should be noted that aseismic creeping, which may have significant consequences on the recurrence intervals, was reported along both San Andreas Fault [e.g., *Schmidt et al.*, 2005; *Titus et al.*, 2006; *Wei et al.*, 2009] and the NAF [e.g., *Çakır et al.*, 2005; 2012].

In summary:

1. Time-stratigraphic correlations, like between Yeniçağa Lake and Sofular Cave, can be a strong tool to improve sediment chronologies;
2. Combination of precise sediment chronology, historical seismicity records, and on-fault paleoseismic trench data is crucial in order to evaluate the seismic origin of lacustrine sedimentary events;
3. The possible bimodal recurrence behavior observed in the Yeniçağa sedimentary sequence should be further tested by means of longer cores from this lake and other fault-bounded basins along the NAF.

References

Ambraseys, N. (2009), *Earthquakes in the Mediterranean and Middle East - A multidisciplinary study of seismicity up to 1900*, Cambridge Univ. Press, Cambridge.

Ambraseys, N., and J. Jackson (1998), Faulting associated with historical and recent earthquakes in the eastern Mediterranean region, *Geophys. J. Int.*, *133*, 390–406.

Arca, S. (2004), Neotectonics and evolution of the Yeniçağa Basin, Bolu - Turkey, MS thesis, Dep. of Geol. Engineering, Middle East Technical University, Ankara, Turkey.

Avsar, U. (2013), Lacustrine paleoseismic records from the North Anatolian Fault, Turkey, PhD thesis, Ghent University, Gent, Belgium.

Beck, C. (2009), Late Quaternary lacustrine paleoseismic archives in north-western Alps: Examples of earthquake-origin assessment of sedimentary disturbances, *Earth Sci. Rev.*, *96*, 327–344, doi:10.1016/j.earscirev.2009.07.005.

Ben-Menahem, A. (1976), Dating historical earthquakes by mud profiles of lake-bottom sediments, *Nature*, *262*, 200–202, doi:10.1038/262200a0.

Bertrand, S., L. Doner, S. Akçer Ön, U. Sancar, U. Schudack, S. Mischke, M. N. Çagatay, and S. A. G. Leroy (2011), Sedimentary record of coseismic subsidence in Hersek coastal lagoon (Izmit Bay, Turkey) and the late Holocene activity of the North Anatolian Fault, *Geochem. Geophys. Geosyst.*, *12*, Q06002, doi:10.1029/2011GC003511.

Boes, X., S. B. Moran, J. King, M. N. Cagatay, and A. Hubert-Ferrari (2010), Records of large earthquakes in lake sediments along the North Anatolian Fault Turkey, *J. Paleolimnol.*, *43*, 901–920, doi:10.1007/s10933-009-9376-x.

Bommer, J. J., and C. E. Rodriguez (2002), Earthquake-induced landslides in Central America, *Eng. Geol.*, *63*, 189–220, doi:10.1016/S0013-7952(01)00081-3.

Bronk Ramsey, C. (2007), OxCal Program v. 4.0.5: University of Oxford, Radiocarbon Accelerator unit.

Çakır, Z., A. M. Akoğlu, S. Belabbes, S. Ergintav, and M. Meghraoui (2005), Creeping along the İsmetpaşa section of the North Anatolian Fault (Western Turkey): Rate and extent from InSAR, *Earth Planet. Sci. Lett.*, *238*, 225–234, doi:10.1016/j.epsl.2005.06.044.

Çakır, Z., S. Ergintav, H. Özener, U. Doğan, A. M. Akoğlu, M. Meghraoui, and R. Reilinger (2012), Onset of aseismic creep on major strike-slip faults, *Geology*, *40*, 1115–1118, doi:10.1130/G33522.1.

Dadson, S. J., et al. (2004), Earthquake triggered increase in sediment delivery from an active mountain belt, *Geology*, *32*, 733–736, doi:10.1130/G20639.1.

Dypvik, H., and N. B. Harris (2001), Geochemical facies analysis of fine-grained siliciclastics using Th/U, Zr/Rb and (Zr + Rb)/Sr ratios, *Chem. Geol.*, *181*, 131–146, doi:10.1016/S0009-2541(01)00278-9.

Fleitmann, D., et al. (2009), Timing and climatic impact of Greenland interstadials recorded in stalagmites from northern Turkey, *Geophys. Res. Lett.*, *36*, L19707, doi:10.1029/2009GL040050.

Fraser, J., K. Vanneste, and A. Hubert-Ferrari (2010), Recent behavior of the North Anatolian Fault: Insights from an integrated paleoseismological data set, *J. Geophys. Res.*, *115*, B09316, doi:10.1029/2009JB006982.

Gutdeutsch, R., and C. Hammerl (1999), An uncertainty parameter of historical earthquakes – the record threshold, *J. Seismol.*, *3*, 351–362, doi:10.1023/A:1009818413087.

Hartleb, R. D., J. F. Dolan, Ö. Kozacı, H. S. Akyüz, and G. G. Seitz (2006), A 2500-yr-long paleoseismologic record of large, infrequent earthquakes on the North Anatolian Fault at Çukurçimen, Turkey, *Geol. Soc. Am. Bull.*, *118*(7), 823–840, doi:10.1130/B25838.1.

Howarth, J. D., S. J. Fitzsimons, R. J. Norris, and G. E. Jacobsen (2012), Lake sediments record cycles of sediment flux driven by large earthquakes on the Alpine fault, New Zealand, *Geology*, *40*(12), 1091–1094, doi:10.1130/G33486.1.

Hubert-Ferrari, A., R. Armijo, G. King, B. Meyer, and A. A. Barka (2002), Morphology, Displacement, and Slip-rates along North Anatolian Fault, Turkey, *J. Geophys. Res.*, *107*(B10), 2235, doi:10.1029/2001JB000393.

Kagan, E., M. Stein, A. Agnon, and F. Neumann (2011), Intrabasin paleoearthquake and quiescence correlation of the late Holocene Dead Sea, *J. Geophys. Res.*, *116*, B04311, doi:10.1029/2010JB007452.

Keefer, D. K. (1984), Landslides caused by earthquakes, *Geol. Soc. Am. Bull.*, *95*, 406–421.

Keefer, D. K. (1994), The importance of earthquake-induced landslides to longterm slope erosion and slope-failure hazards in seismically active regions, *Geomorphology*, *10*, 265–284, doi:10.1016/0169-555X(94)90021-3.

Keefer, D. K., and M. E. Moseley (2004), Southern Peru desert shattered by the great 2001 earthquake: Implications for paleoseismic and paleo-El Nino–Southern Oscillation records, *Proc. Natl. Acad. Sci. U. S. A.*, *101*, 10,878–10,883, doi:10.1073/pnas.0404320101.

Kondo, H., Y. Awata, O. Emre, A. Dogan, S. Ozalp, F. Tokay, C. Yıldırım, T. Yoshioka, and K. Okumura (2005), Slip distribution, fault geometry, and fault segmentation of the 1944 Bolu-Gerede earthquake rupture North Anatolian Fault, Turkey, *Bull. Seismol. Soc. Am.*, *95*, 1234–1249, doi:10.1785/0120040194.

Kondo, H., V. Özaksoy, and C. Yıldırım (2010), Slip history of the 1944 Bolu-Gerede earthquake rupture along the North Anatolian fault system: Implications for recurrence behavior of multisegment earthquakes, *J. Geophys. Res.*, *115*, B04316, doi:10.1029/2009JB006413.

Kozacı, Ö. (2008), Constancy of strain release rates along the North Anatolian Fault, PhD thesis, University of Southern California, Los Angeles.

Kylander, M. E., L. Ampel, B. Wohlfarth, and D. Veres (2011), High-resolution X-ray fluorescence core scanning analysis of Les Echets (France) sedimentary sequence: new insights from chemical proxies, *J. Quat. Sci.*, *26*, 109–117, doi:10.1002/jqs.1438.

Leroy, S. A. G., S. Boyraz, and A. Gürbüz (2009), High-resolution palynological analysis in Lake Sapanca as a tool to detect recent earthquakes on the North Anatolian Fault, *Quat. Sci. Rev.*, *28*, 2616–2632, doi:10.1016/j.quascirev.2009.05.018.

Leroy, S. A. G., M. J. Schwab, and P. J. M. Costa (2010), Seismic influence on the last 1500-year infill history of Lake Sapanca (North Anatolian Fault, NW Turkey), *Tectonophysics*, *486*, 15–27, doi:10.1016/j.tecto.2010.02.005.

Lienkaemper, J. J., and C. Bronk Ramsey (2009), OxCal: Versatile tool for developing paleoearthquake chronologies - a primer, *Seismol. Res. Lett.*, *80*, 431–434, doi:10.1785/gssrl.80.3.431.

Malamud, B. D., D. L. Turcotte, F. Guzzetti, and P. Reichenbach (2004), Landslides, earthquakes, and erosion, *Earth Planet. Sci. Lett.*, *229*(1-2), 45–59, doi:10.1016/j.epsl.2004.10.018.

Marco, S., M. Stein, A. Agnon, and H. Ron (1996), Long-term earthquake clustering: A 50,000-year paleoseismic record in the Dead Sea Graben, *J. Geophys. Res.*, *101*, 6179–6191, doi:10.1029/95JB01587.

Moernaut, J., M. De Batist, F. Charlet, K. Heirman, E. Chapron, M. Pino, R. Brümmer, and R. Urrutia (2007), Giant earthquakes in South-Central Chile revealed by Holocene mass-wasting events in Lake Puyehue, *Sediment. Geol.*, *195*, 239–256, doi:10.1016/j.sedgeo.2006.08.005.

Monecke, K., F. S. Anselmetti, A. Becker, M. Schnellmann, M. Sturm, and D. Giardini (2006), Earthquake-induced deformation structures in lake deposits: a late Pleistocene to Holocene Paleoseismic record for Central Switzerland, *Eclogae Geol. Helv.*, *99*, 343–362, doi:10.1007/s00015-006-1193-x.

Nasir, A., W. Lenhardt, E. Hintersberger, and K. Decker (2013), Assessing the completeness of historical and instrumental earthquake data in Austria and the surrounding areas, *Austrian J. Earth Sci.*, *106*(1), 90–102.

Nur, A., and E. H. Cline (2000), Poseidon's horses: Plate tectonics and earthquake storms in the Late Bronze Age Aegean and eastern Mediterranean, *J. Archaeol. Sci.*, *27*, 43–63, doi:10.1006/jasc.1999.0431.

Okumura, K., T. Yoshioka, and I. Kuşçu (1993), Surface faulting on the North Anatolian fault in these two millennia, *U.S. Geol. Surv. Open File Rep.*, *94-568*, 143–144.

Reilinger, R., et al. (2006), GPS constraints on continental deformation in the Africa-Arabia-Eurasia continental collision zone and implications for the dynamics of plate interactions, *J. Geophys. Res.*, *111*, B05411, doi:10.1029/2005JB004051.

Reimer, P. J., et al. (2004), IntCal04 terrestrial radiocarbon age calibration, 0–26 Ka cal BP, *Radiocarbon*, *46*, 1029–1058.

Rockwell, T. K., K. Okumura, T. Duman, D. Ragona, G. Seitz, Y. Awata, G. U. Arku, E. Aksoy, M. Ferry, and M. Meghraoui (2006), Paleoseismology of the 1912, 1944 and 1999 ruptures on the North Anatolian fault: Implications for late Holocene patterns of strain release, *International workshop on comparative studies of the North Anatolian Fault* (*Northwest Turkey*) *and the San Andreas Fault* (*Southern California*), *Istanbul Technical University*, *Abstracts*, *1*, 11-13.

Rodriguez, C. E., J. J. Bommer, and R. J. Chandler (1999), Earthquake induced landslides: 1980–1997, *Soil Dyn. Earthquake Eng.*, *18*, 325–346, doi:10.1016/S0267-7261(99)00012-3.

Schmidt, D. A., R. Bürgmann, R. M. Nadeau, and M. d'Alessio (2005), Distribution of aseismic slip rate on the Hayward fault inferred from seismic and geodetic data, *J. Geophys. Res.*, *110*, B08406, doi:10.1029/2004JB003397.

Schwab, M. J., P. Werner, P. Dulski, E. McGee, N. R. Nowaczyk, S. Bertrand, and S. A. G. Leroy (2009), Palaeolimnology of Lake Sapanca and identification of historic earthquake signals, Northern Anatolian Fault Zone (Turkey), *Quat. Sci. Rev.*, *28*, 991–1005, doi:10.1016/j.quascirev.2009.02.018.

Stein, R. S., A. A. Barka, and J. H. Dieterich (1997), Progressive failure on the North Anatolian fault since 1939 by earthquake stress triggering, *Geophys. J. Int.*, *128*, 594–604, doi:10.1111/j.1365-246X.1997.tb05321.x.

Strasser, M., K. Monecke, M. Schnellmann, and F. S. Anselmetti (2013), Lake sediments as natural seismographs: A compiled record of Late Quaternary earthquakes in Central Switzerland and its implication for Alpine deformation, *Sedimentology*, *60*, 319–341, doi:10.1111/sed.12003.

Titus, S. J., C. DeMets, and B. Tikoff (2006), Thirty-five-year creep rates for the creeping segment of the San Andreas Fault and the effects of the 2004 Parkfield earthquake: Constraints from alignment arrays, continuous Global Positioning System, and creepmeters, *Bull. Seismol. Soc. Am.*, *96*, S250–S268, doi:10.1785/0120050811.

Urban, N. R. (1994), Retention of Sulfur in lake sediments, in *Environmental Chemistry of Lakes and Reservoirs*, edited by L. A. Baker, pp. 323–369, American Chemical Society, Washington, D. C.

Wei, M., D. Sandwell, and Y. Fialko (2009), A Silent M4.8 Slip Event of October 3-6, 2006, on the Superstition Hills Fault, Southern California, *J. Geophys. Res.*, *114*, B07402, doi:10.1029/2008JB006135.

Weldon, R., K. Scharer, T. Fumal, and G. Biasi (2004), Wrightwood and the earthquake cycles: What a long recurrence record tells us about how faults work, *GSA Today*, *14*, 4–10.

Wronkiewicz, D. J., and K. C. Condie (1989), Geochemistry and provenance of sediments from the Pangola Supergroup, South Africa: Evidence for a 3.0 Ga-old continental craton, *Geochim Cosmochim. Acta*, *53*, 1537–1549.